

# Computing Sparse Representation in a Highly Coherent Dictionary Based on Difference of $L_1$ and $L_2$

Yifei Lou, Penghang Yin, Qi He and Jack Xin \*

## Abstract

We study analytical and numerical properties of the  $L_1 - L_2$  minimization problem for sparse representation of a signal over a highly coherent dictionary. Though the  $L_1 - L_2$  metric is non-convex, it is Lipschitz continuous. The difference of convex algorithm (DCA) is readily applicable for computing the sparse representation coefficients. The  $L_1$  minimization appears as an initialization step of DCA. We further integrate DCA with a non-standard simulated annealing (SA) methodology to approximate globally sparse solutions. Non-Gaussian random perturbations are more effective than standard Gaussian perturbations for improving sparsity of solutions. In numerical experiments, we conduct an extensive comparison among sparse penalties such as  $L_0, L_1, L_p$  for  $p \in (0, 1)$  based on data from three specific applications (over-sampled discrete cosine basis, differential absorption optical spectroscopy, and image denoising) where highly coherent dictionaries arise. We find numerically that the  $L_1 - L_2$  minimization persistently produces better results than  $L_1$  minimization, especially when the sensing matrix is ill-conditioned. In addition, the DCA method outperforms many existing algorithms for other nonconvex metrics.

---

\*Department of Mathematics, UC Irvine, Irvine, CA 92697, USA. The work was partially supported by NSF grants DMS-0928427 and DMS-1222507. Manuscript revised on July 19, 2014.

# 1 Introduction

Sparse representation in an overcomplete basis appears frequently in signal processing and imaging applications such as oversampled discrete Fourier transform, Gabor frames, curvelet frames, concatenation of different orthonormal bases [3]. It is known to be related to sparse coding in visual systems [19]. The advantage is robustness and reliability.

Mathematically it amounts to finding the sparsest solution to an under-determined linear system

$$b = Ax + n , \tag{1}$$

where  $b$  is the observed data,  $A$  is a  $M \times N$  ( $M < N$ ) matrix and  $n$  is noise. A fundamental issue in compressed sensing (CS) is how to enforce sparsity when solving the linear system (1). A natural strategy is to minimize  $L_0$  norm,  $\|x\|_0$ , which is the number of nonzero elements. Unfortunately, the  $L_0$  minimization is NP hard [18]. There are two methods that approach  $L_0$  directly. One is the greedy approach, the so called orthogonal matching pursuit (OMP) [23]. Its basic idea is to select one best column from the matrix  $A$  at a time, followed by an orthogonal projection to avoid selecting the same vector multiple times. The other is the penalty decomposition method [17], which solves

$$\min_{x \in \mathbb{R}^N} \frac{1}{2} \|Ax - b\|_2^2 + \lambda \|x\|_0 , \tag{2}$$

by a series of minimization problems with an increasing sequence  $\{\rho^k\}$ :

$$\begin{aligned} (x^{k+1}, y^{k+1}) &= \arg \min \frac{1}{2} \|Ax - b\|^2 + \frac{\rho^k}{2} \|x - y\|^2 + \lambda \|y\|_0 \\ \rho^{k+1} &= \tau \rho^k \quad (\tau > 1) . \end{aligned} \tag{3}$$

In general, the two approaches only provide sub-optimal sparse solutions to the original problem.

The convex relaxation of  $L_1$  in lieu of  $L_0$  attracts considerable attention in CS. There are numerous algorithms, such as LASSO [22], Bregman iterations [27], and alternating direction method of multipliers (ADMM) [2], devoted to solving  $L_1$  regularized problems efficiently and accurately. The theoretical aspect of  $L_1$  relaxation is studied in [5, 8] and elsewhere. A deterministic result in [8] says that exact  $L_1$  recovery is possible if

$$\|x\|_0 < \frac{1 + 1/\mu}{2} , \tag{4}$$

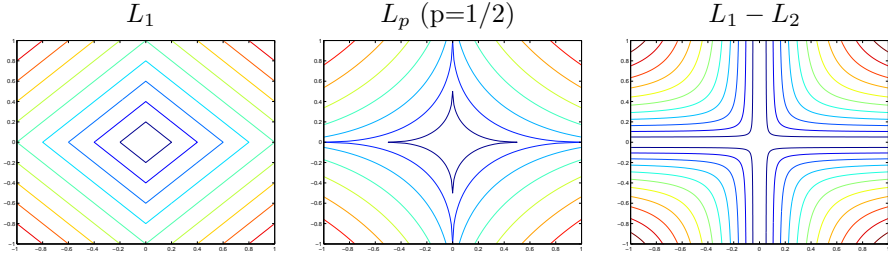


Figure 1: Level lines of three sparsity metrics. Compared with  $L_1$ , the level lines of  $L_p$  and  $L_1 - L_2$  are closer to the axes when minimized (closer to those of  $L_0$ ).

where  $\mu$  is mutual coherence of the matrix  $A = [\mathbf{a}_1, \dots, \mathbf{a}_N]$ , defined as

$$\mu = \max_{i \neq j} \frac{|\mathbf{a}_i^T \mathbf{a}_j|}{\|\mathbf{a}_i\| \|\mathbf{a}_j\|} .$$

The inequality (4) suggests that  $L_1$  may not perform well for highly coherent sensing matrices in that if  $\mu \sim 1$ , then  $\|x\|_0$  can be at most 1. Though the theoretical estimate is far from sharp, we shall show numerical examples of such phenomenon later.

In this paper we study a non-convex but Lipschitz continuous metric  $L_1 - L_2$  for sparse signal recovery in the highly coherent regime of CS, and compare with the concave and Hölder continuous sparsity metric  $L_p$  ( $p \in (0, 1)$ ).

Recently, nonconvex measures, such as  $L_p$  for  $p \in (0, 1)$  in [7],  $L_1/L_2$  and  $L_1 - L_2$  in [10, 25], have been proposed as alternatives to  $L_1$ . As illustrated in Figure 1 in  $\mathbb{R}^2$ , the level curves of  $L_p$  and  $L_1 - L_2$  are closer to  $L_0$  than those of  $L_1$ . Geometrically, minimizing a sparse measure subject to linear constraints is equivalent to finding an interception of an affine subspace (corresponding to solutions of the linear constraints) with a level set of that measure so that the intersection is closest to a coordinate axis/plane. For  $L_p$  and  $L_1 - L_2$ , due to their curved level set, the interception is more likely to occur at the coordinate axis/plane, giving a sparse solution. For  $L_1$ , it is possible that the affine subspace coincides with a segment of a level set (a resonance phenomenon), *i.e.*, any point on that segment is a solution of  $L_1$  minimization. If such resonance occurs,  $L_1$  minimization fails to find a sparse solution. There may be other

degenerate scenarios in three and above dimensions when the sensing matrix is highly coherent.

Though  $L_p$  and  $L_1 - L_2$  measures are theoretically better than  $L_1$  to promote sparsity, the non-convexity poses a challenge to computation. For  $L_p$  minimization, iterative reweighted least-square [7] is considered for the constrained problem, while an unconstrained formulation is discussed in [16]. The minimizing sequence may get stuck at a **stationary point**. The  $L_p$  metric has an a-priori unknown parameter  $p$  and is non-Lipschitz. The  $L_1 - L_2$  is however Lipschitz continuous and free of parameter. It can be minimized by the difference of convex algorithm (DCA) [21] where linearization convexifies the objective without additional smoothing or regularization. The DCA minimizing sequence converges to a stationary point theoretically, **which empirically often (yet not always) turns out to be a global minimizer**. To avoid trapping in a local basin, we further incorporate a variant of the so called simulated annealing (SA) technique in global optimization. Here we found that non-Gaussian random perturbations are better at improving sparsity of solutions than standard Gaussian perturbations. A hybrid method integrating SA for  $L_p$  minimization is discussed in [24].

The rest of the paper is organized as follows. In Section 2.1, we show a toy example when  $L_1$  minimization fails to find the sparsest solution, while  $L_p$  and  $L_1 - L_2$  minimization succeed. In Section 2.2, we then present some nice properties of  $L_1 - L_2$  metric as a sparsity measure. In Section 3, we discuss the algorithms for computing sparse representation based on  $L_1 - L_2$  minimization, where both constrained and unconstrained formulations are given. In order to find a global solution, we further integrate DCA and the simulated annealing method. As numerical experiments, we investigate three specific applications (over-sampled discrete cosine transform, optical spectroscopy, and image denoising) where highly coherent matrices are encountered. We demonstrate that  $L_1 - L_2$  minimization with DCA solver is robust in finding sparse solutions, and outperforms some state-of-the-art algorithms. Finally, discussion and conclusion are given in Section 5.

## 2 Sparsity measures

### 2.1 A toy example

We study a toy example where  $L_1$  fails to find the sparsest solution, while both  $L_1 - L_2$  and  $L_p$  can. Consider a linear system

$$\begin{bmatrix} 2 & 1 & 0 \\ 1 & 1 & 1 \\ 0 & 1 & 2 \end{bmatrix} x = \begin{bmatrix} 1 \\ 1 \\ 1 \end{bmatrix} \quad (5)$$

The sparsest solution is  $x_0 = [0, 1, 0]^T$ . We find any vector of form  $[a, 1 - 2a, a]^T$  for  $a \in [0, 0.5]$  is a solution of  $L_1$  minimization subject to (5). In other words,  $L_1$  fails to pick up the sparsest solution.

$L_p$  minimization is equivalent to minimizing  $2a^p + (1 - 2a)^p$  for  $a \in [0, 0.5]$ . As  $L_p$  is concave, the minimum is attained at the boundary. Consequently, we only need to evaluate  $a = 0$  and  $a = 0.5$  to see which one is smaller. By simple calculations,  $L_p$  attains its minimum at  $a = 0$  for  $p < 1$ . In other words,  $L_p$  minimization yields the sparsest solution.

Let us look at  $L_1 - L_2$ . A non-zero vector is 1-sparse (only one non-zero element) if and only if its  $L_1 - L_2$  is 0. Since  $x_0$  is 1-sparse, then only 1-sparse vectors could be the solution of minimizing  $L_1 - L_2$  subject to (5). But the other 1-sparse vectors do not satisfy the linear equation, and as a result we can get  $x_0$  exactly if minimizing  $L_1 - L_2$ .

### 2.2 Theoretical properties of $L_1 - L_2$

To make this paper self-contained, we list some nice properties of  $L_1 - L_2$ . Please refer to [26] for the proof. Recall that the well-known restricted isometry property (RIP) [5] in compressive sensing is that for all subsets  $T \subset \{1, \dots, N\}$  with its cardinality  $|T| \leq S$ ,

$$(1 - \delta_S)\|x\|_2^2 \leq \|A_T x\|_2^2 \leq (1 + \delta_S)\|x\|_2^2 \quad \forall x \in \mathbb{R}^N,$$

where  $A_T$  is a submatrix of  $A$  with column indices  $T$ , and  $\delta_S$  is a parameter depending on  $S$ . The RIP condition for  $L_1 - L_2$  exact recovery is given in the following.

**Theorem 2.1** *Let  $x_0$  be any vector with sparsity of  $s$  and  $b = Ax_0$ . Suppose that the following condition holds*

$$\delta_{3s} + a(s)\delta_{4s} < a(s) - 1, \quad (6)$$

where

$$a(s) = \left( \frac{\sqrt{3s} - 1}{\sqrt{s} + 1} \right)^2,$$

then  $x_0$  is the unique solution to a constrained minimization problem:

$$\min_{x \in \mathbb{R}^N} \|x\|_1 - \|x\|_2 \quad \text{subject to} \quad Ax = b. \quad (7)$$

In fact, Theorem 2.1 does not characterize  $L_1 - L_2$  completely, as in practice its assumption can be further relaxed. Due to concavity of the metric, we can prove that even local minimizers of (7) satisfy certain sparsity, no matter whether  $A$  satisfies RIP or not.

**Theorem 2.2** *Let  $x^*$  be a local minimizer of the constrained problem (7) then  $A|_{\Lambda^*}$  is of full column rank, i.e. the columns of  $A|_{\Lambda^*}$  are linearly independent.*

The same result can be obtained for the unconstrained problem:

$$\min_{x \in \mathbb{R}^N} \frac{1}{2} \|Ax - b\|_2^2 + \lambda(\|x\|_1 - \|x\|_2) \quad (8)$$

**Corollary 2.1** *Let  $x^*$  be a local minimizer of (8) then the columns of  $A|_{\Lambda^*}$  are linearly independent.*

By Theorem 2.2 and Corollary 2.1, we readily conclude the following facts:

- (a) Suppose  $x^*$  is a local minimizer of (7) or (8) and  $A \in \mathbb{R}^{M \times N}$  is of full row rank, i.e.  $\text{rank}(A) = M$ , then the sparsity of  $x^*$  is at most  $M$ .
- (b) **If  $x^*$  is a local minimizer of (7), then there is no such  $x \in \mathbb{R}^N$  satisfying  $Ax = b$  and  $\text{support}(x) \subseteq \Lambda^*$ , i.e. it is impossible to find a feasible solution whose support is contained in  $\Lambda^*$ .**
- (c) The number of the local minimizers of (7) or (8) is finite.

### 3 Algorithm

To compute sparse representation based on  $L_1 - L_2$ , both constrained and unconstrained minimization problems are discussed in Section 3.1 and Section 3.2 respectively. In Section 3.3, we further employ a simulated annealing technique to search for global solutions of these two nonconvex problems.

#### 3.1 Unconstrained minimization

We start with the unconstrained minimization problem (8). We adopt a difference of convex algorithm (DCA), which is to decompose  $F(x) = G(x) - H(x)$ , where

$$\begin{cases} G(x) = \frac{1}{2}\|Ax - b\|_2^2 + \lambda\|x\|_1 \\ H(x) = \lambda\|x\|_2 \end{cases} \quad (9)$$

By linearizing  $H$ , we can design an iterative scheme that starts with  $x^1 \neq \mathbf{0}$ ,

$$x^{n+1} = \arg \min_{x \in \mathbb{R}^N} \frac{1}{2}\|Ax - b\|_2^2 + \lambda\|x\|_1 - \langle x - x^n, \lambda \frac{x^n}{\|x^n\|_2} \rangle \quad (10)$$

To advance to a new solution, it requires solving a  $L_1$  regularized subproblem of the form

$$\min_{x \in \mathbb{R}^N} \frac{1}{2}x^T(A^T A)x + z^T x + \lambda\|x\|_1, \quad (11)$$

where  $z = A^T b + \lambda \frac{x^n}{\|x^n\|_2}$ . We consider the augmented Lagrangian

$$L_\delta(x, y, u) = \frac{1}{2}x^T(A^T A)x + z^T x + \lambda\|y\|_1 + u^T(x - y) + \frac{\delta}{2}\|x - y\|_2^2.$$

ADMM iterates between minimizing  $L_\delta$  with respect to  $x$ , minimizing with respect to  $y$  and updating  $u$ . The pseudo-code of solving the unconstrained  $L_1 - L_2$  minimization is described in Algorithm 1.

In our experiments we always set the initial value  $x^1$  as the solution of unconstrained  $L_1$  problem, that is to solve (11) with  $z = \mathbf{0}$ . So basically we are minimizing  $L_1 - L_2$  on top of  $L_1$ . In practice the algorithm takes only a few steps to convergence. Theoretically, we can prove that the sequence  $\{x^n\}$  is bounded and  $\|x^{n+1} - x^n\|_2 \rightarrow 0$ , thus limit points of  $\{x^n\}$  are stationary points of (8) satisfying the first-order optimality condition.

---

**Algorithm 1** A DCA method for unconstrained  $L_1 - L_2$  minimization

---

Define  $\epsilon_{outer} > 0, \epsilon_{inner} > 0$  and initialize  $x^0 = \mathbf{0}, x^1 \neq \mathbf{0}, n = 1$

**while**  $\|x^n - x^{n-1}\| > \epsilon_{outer}$  **do**

Let  $z = \frac{x^n}{\|x^n\|_2}$  and  $x_0 = \mathbf{0}, x_1 = x^n, i = 1, y_i = x_i, u_i = \mathbf{0}$

**while**  $\|x_i - x_{i-1}\| > \epsilon_{inner}$  **do**

$$x_{i+1} = (A^T A + \delta I)^{-1}(\delta y_i - z - u_i)$$

$$y_{i+1} = \mathit{shrink}(x_{i+1} + u_i/\delta, \lambda/\delta)$$

$$u_{i+1} = u_i + \delta(x_{i+1} - y_{i+1})$$

$$i = i + 1$$

**end while**

$$n = n + 1$$

$$x^n = x_i$$

**end while**

---

**Theorem 3.1** Let  $F(x) = \frac{1}{2}\|Ax - b\|_2^2 + \lambda(\|x\|_1 - \|x\|_2)$  with the D.C. decomposition in (9) and  $\{x^n\}$  be the sequence of iterates generated by Algorithm 1, then

- (a)  $F(x) \rightarrow \infty$  as  $\|x\|_2 \rightarrow \infty$ . so the level set  $\{x \in \mathbb{R}^N : F(x) \leq F(x^0)\}$  is bounded.
- (b)  $F(x^n) - F(x^{n+1}) \geq 2c\|x^{n+1} - x^n\|_2^2$  and thus  $\|x^{n+1} - x^n\|_2 \rightarrow 0$ .
- (c) Any limit point  $x^* \neq \mathbf{0}$  of  $\{x^n\}$  satisfies the first-order optimality condition

$$A^T(Ax^* - b) + \lambda(w^* - \frac{x^*}{\|x^*\|_2}) = \mathbf{0}, \quad \text{for some } w^* \in \partial\|x^*\|_1, \quad (12)$$

which means  $x^*$  is a stationary point of (8).

Starting from (12), we obtain the following results.

**Theorem 3.2**  $\forall k \geq 1$ , we can choose a regularization parameter  $\lambda_k > 0$  for (8) so that  $\|x^*\|_0 \leq k$ .

Theorem 3.2 suggests that we can control the sparsity of the limit point of the DCA algorithm by choosing a proper  $\lambda$ . Please refer to [26] for the proof of both theorems.

### 3.2 Constrained minimization

For the constrained problem (7), we apply a similar trick as the unconstrained problem by considering the following iterative scheme

$$\begin{aligned} x^{n+1} &= \arg \min \|x\|_1 - \left\langle \frac{x^n}{\|x^n\|_2}, x \right\rangle \\ &\text{s.t. } Ax = b \end{aligned} \quad (13)$$

Each subproblem (13) amounts to solving a constrained  $L_1$  minimization,

$$\min |x| - z^T x \quad \text{s.t. } Ax = b, \quad (14)$$

for  $z = \frac{x^n}{\|x^n\|_2}$ . To solve (14), we introduce two Lagrange multipliers  $u, v$  and define an augmented Lagrangian

$$L_\delta(x, y, u, v) = \|y\|_1 - z^T x + u^T(x - y) + v^T(Ax - b) + \frac{\delta}{2}\|x - y\|^2 + \frac{\delta}{2}\|Ax - b\|^2,$$

for  $\delta > 0$ . ADMM finds a saddle point

$$L_\delta(x^*, y^*, u, v) \leq L_\delta(x^*, y^*, u^*, v^*) \leq L_\delta(x, y, u^*, v^*) \quad \forall x, y, u, v$$

by alternately minimizing  $L_\delta$  with respect to  $x$ , minimizing with respect to  $y$  and updating the dual variables  $u$  and  $v$ . The saddle point  $(x^*, y^*)$  will be a solution to (14) and we can take  $x^*$  be the solution to (13), *i.e.*,  $x^{n+1} = x^*$ . The overall algorithm for solving the constrained  $L_1 - L_2$  is described in Algorithm 2.

### 3.3 Simulated Annealing

The DCA method does not guarantee a global minimum in general. We further employ a technique, called simulated annealing (SA), to traverse a **stationary point** to a global solution. SA has drawn much attentions dealing with global optimization. There are many generic SA algorithms, see Kirkpatrick [15], Geman and Geman [13], Gidas [14], and the reference therein. In addition, Carnevali *et. al.* [6] apply this technique to many applications in image processing.

Here is a brief description of simulated annealing. The term ‘‘annealing’’ is analogous to the cooling of a liquid or solid in a physical system. Consider the problem of minimizing the cost function  $f(x)$ . Simulated annealing algorithm

---

**Algorithm 2** A DCA method for constrained  $L_1 - L_2$  minimization

---

Define  $\epsilon_{outer} > 0, \epsilon_{inner} > 0$  and initialize  $x^0 = \mathbf{0}, x^1 \neq \mathbf{0}, n = 1$

**while**  $\|x^n - x^{n-1}\| > \epsilon_{outer}$  **do**

Let  $z = \frac{x^n}{\|x^n\|_2}$  and  $x_0 = \mathbf{0}, x_1 = x^n, i = 1, y_i = x_i, u_i = v_i = \mathbf{0}$

**while**  $\|x_i - x_{i-1}\| > \epsilon_{inner}$  **do**

$$x_{i+1} = (A^T A + \mathbf{I})^{-1}(A^T b + y_i + (z - u_i - A^T v_i)/\delta)$$

$$y_{i+1} = \mathit{shrink}(x_{i+1} + u_i/\delta, 1/\delta)$$

$$u_{i+1} = u_i + \delta(x_{i+1} - y_{i+1})$$

$$v_{i+1} = v_i + \delta(Ax_{i+1} - b)$$

$$i = i + 1$$

**end while**

$$n = n + 1$$

$$x^n = x_i$$

**end while**

---

begins with an initial solution and iteratively generates new ones, each of which is randomly selected among the “neighborhood” of the previous state. If the new solution is better than the previous one, it is accepted; otherwise, it is accepted with certain probability. The probability of accepting a new state is given by  $\exp(-\frac{f_{new} - f_{curr}}{T}) > R$ , where  $R$  is a random number between 0 and 1, and  $T$  is a temperature parameter. The algorithm usually starts with a high temperature, and then gradually goes down to 0. The cooling must be slow enough so that the system does not get stuck into **saddle points or** local minima of  $f(x)$ .

There are two important aspects in implementing simulated annealing. One is how to lower the temperature  $T$ . Kirkpatrick *et. al.* [15] suggest  $T$  decays geometrically in the number of cooling phases. Geman and Geman [13] prove that if  $T$  decreases at the rate of  $\frac{1}{\log k}$ , where  $k$  is the number of iterations, then the probability distribution for the algorithm converges to the uniform distribution over all the global minimum points. In our algorithm, we follow Geman and Geman’s suggestion by decreasing  $T$  at the rate of  $\frac{1}{\log k}$ . Another aspect is how to advance to a new state based on the current one. One of the most common methods is to add Gaussian random noise. However, due to the presence of a large number of **saddle points and** local minima, this

perturbation method yields slow convergence of the SA algorithm. To overcome this difficulty, we propose two perturbative strategies. Together with Gaussian perturbation, we list the three SA methods as follows,

- SA1. Define the support set of a vector  $x$  by  $support(x) := \{i | x_i \neq 0\}$ . We randomly choose the new state  $x_{new}$  such that  $support(x_{new}) \subset support(x_{curr})$  and  $|x_{new}|_0 < |x_{curr}|_0$ .
- SA2. We randomly choose the new state  $x_{new}$  such that  $|x_{new}|_0 < \gamma |x_{curr}|_0$  with some constant  $\gamma < 1$ .
- SA3. We choose the new state  $x_{new}$  by Gaussian perturbations, i.e.  $x_{new} = x_{curr} + \text{Gaussian noise}$ .

The idea of SA1 and SA2 is to help maintain the monotone (non-increasing) sparsity property of the iterates. The pseudo-code of the SA method in combination of DCA is given in Algorithm 3.

## 4 Applications

In this section we examine three specific applications where the sensing matrix is highly coherent. They are compressive sensing based on oversampled DCT matrices, wavelength misalignment in differential optical absorption spectroscopy (DOAS) analysis, and image denoising via sparse representation in an overcomplete dictionary. For each problem, we compare the proposed method for minimizing  $L_1 - L_2$  with some state-of-the-art algorithms for  $L_0, L_1$ , and  $L_p$ . Experiments show promising results of using  $L_1 - L_2$  as a sparse measure and solving sparse coefficients by DCA and SA.

### 4.1 Over-sampled DCT

We consider an over-sampled DCT matrix  $A = [\mathbf{a}_1, \dots, \mathbf{a}_N] \in \mathbb{R}^{M \times N}$  with

$$\mathbf{a}_j = \frac{1}{\sqrt{N}} \cos\left(\frac{2\pi \mathbf{w} j}{F}\right), j = 1, \dots, N \quad (15)$$

where  $\mathbf{w}$  is a random vector of length  $M$ . This matrix is derived from the problem of spectral estimation [11] in signal processing, if we replace the cosine

---

**Algorithm 3** L1-L2 DCA with simulated annealing

---

Define  $x_{curr}, x_{new}, \epsilon, T\gamma < 1, \text{maxIter}$  and  $\text{AcceptMax}, \text{Accept} = 0$ .

**while**  $T > \epsilon$  or  $k \leq \text{maxIter}$  **do**

SA1:  $x_{new} = \text{randsample}(x_{curr})$  such that  $\text{support}(x_{new}) \subset \text{support}(x_{curr})$   
and  $|x_{new}|_0 < |x_{curr}|_0$ .

SA2:  $x_{new} = \text{randsample}(x_{curr})$  such that  $|x_{new}|_0 < \gamma|x_{curr}|_0$ , with  $\gamma < 1$ .

SA3:  $x_{new} = x_{curr} + \text{Gaussian noise}$ .

Update  $x_{new}$  by the DCA solution of  $L_1 - L_2$  using  $x_{new}$  as initial guess

**if**  $f(x_{new}) \leq f(x_{curr})$  **then**

$x_{curr} = x_{new}$

**else**

**if**  $\exp(-\frac{f(x_{new})-f(x_{curr})}{T}) > \text{rand}(1)$  **then**

$x_{curr} = x_{new}$

**end if**

**end if**

$k = k + 1$

$\text{Accept} = \text{Accept} + 1$

**if**  $\text{Accept} \geq \text{AcceptMax}$  **then**

$T = \frac{1}{\log k}$

$\text{Accept} = 0$

**end if**

**end while**

---

function in (15) by exponential. The matrix is highly coherent. For a  $100 \times 1000$  matrix with  $F = 10$ , the coherence is .9981, while the coherence of a same size matrix with  $F=20$  is .9999.

The sparse recovery under such matrices is possible only if the non-zero elements of solution  $x$  are sufficiently separated. This phenomenon is characterized as *minimum separation* in [4], and this minimum length is referred as the Rayleigh length (RL). The value of RL in (15) is equal to  $F$ . It is closely related to the coherence in the sense that larger  $F$  corresponds to larger coherence of a matrix. We find empirically that at least  $2\text{RL}$  is necessary to ensure optimal sparse recovery. Intuitively, we need sparse spikes to be further apart for more

coherent matrices.

Under the assumption of sparse signal with 2RL separated spikes, we compare algorithms in terms of success rate. Denote  $x_r$  as a reconstructed solution by a certain algorithm. We consider the algorithm successful, if the relative error of  $x_r$  to the ground truth  $x_g$  is less than .001, *i.e.*,  $\frac{\|x_r - x_g\|}{\|x_g\|} < .001$ . The success rate is based on 100 random realizations.

We first investigate the unconstrained algorithms for sparse penalties  $L_1 - L_2, L_1, L_p$  ( $p=1/2$ ) and a **direct  $L_0$  solver, penalty decomposition (3)**. The unconstrained  $L_p$  minimization is solved by Lai *et. al.* in [16]. The sensing matrix is of size  $100 \times 1000$ . The success rate of each measure is plotted in Figure 2. For smaller  $F = 5$ , each measure performs relatively well. When  $F = 20$ , which corresponds to highly coherent matrices, the proposed  $L_1 - L_2$  outperforms  $L_1$  and  $L_p$  for  $p = 1/2$ . For both cases,  $L_1 - L_2$  is consistently better than  $L_1$ .

Figure 3 illustrates that the success rate of  $L_1 - L_2$  increases with the help of SA. The matrix size is  $100 \times 1500$  and  $F = 20$ . We also compare three different random generations of the new state, referred to as SA1-SA3 in Algorithm 3. All of these SA methods can improve the accuracy of the original DCA algorithm for  $L_1 - L_2$  minimization. Both of SA1 and SA2 have better performance than the regular Gaussian perturbation method SA3. Apparently, SA2 has the best performance out of the three, especially when the number of non-zero elements is large.

For the constrained versions of each measure, we observe the similar behavior compared to the unconstrained ones. The plots are presented in Figure 4 for matrices of size  $100 \times 1000$ . The iterative reweighed least square [7] is applied to solve the constrained  $L_p$ .  $L_1 - L_2$  is the best for both incoherent and coherent matrices.

We further look at the success rates of  $L_1 - L_2$  with different combinations of sparsity and RL. The rates are recorded in Table 1, which shows it is possible to deal with large RL, but with the sacrifice of high sparsity, or small number of non-zero elements.

**The computation time for each method is listed in Table 2. The reported time is the average of 100 realizations. Since all the noncon-**

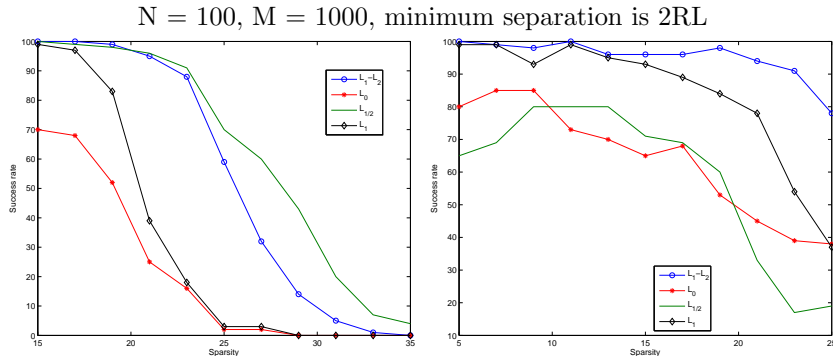


Figure 2: Plots of success rates as a function of sparsity for  $F = 5$  (left) and  $F = 20$  (right). Each metric is solved in an unconstrained optimization framework.

sparsity	6	9	12	15	18	21	24
1RL	100	100	100	97	85	37	3
2RL	100	100	100	100	88	44	11
3RL	100	100	100	99	90	41	8
4RL	100	100	100	98	85	46	8

Table 1: The success rates (%) of  $L_1 - L_2$  for different combinations of sparsity and minimum separation.

**vex optimization methods**  $L_0, L_p, L_1 - L_2$  use the  $L_1$  solution as initial guess, we add  $L_1$  run time on top of each of them. Our  $L_1 - L_2$  method is slower than  $L_p$ , but with better accuracy.

## 4.2 DOAS

Differential optical absorption spectroscopy (DOAS) analysis [20] is a technique that uses Beer’s law to estimate chemical contents and concentrations of a mixture of gases by decomposing a measured characteristic absorption spectra of all the gases into a set of individual ones. A mathematical model is to estimate fitting coefficients  $\{a_j\}$  from a linear model  $J(\lambda) = \sum_j^M a_j \cdot y_j(\lambda) + \eta(\lambda)$ , where the data  $J(\lambda)$  and reference spectra  $\{y_j(\lambda)\}$  are given at each wavelength  $\lambda$  and  $\eta(\lambda)$  is noise. A challenging complication in practice is wavelength misalignment, *i.e.*,

$N = 100, M = 1500, F = 20$ , minimum separation is 2RL

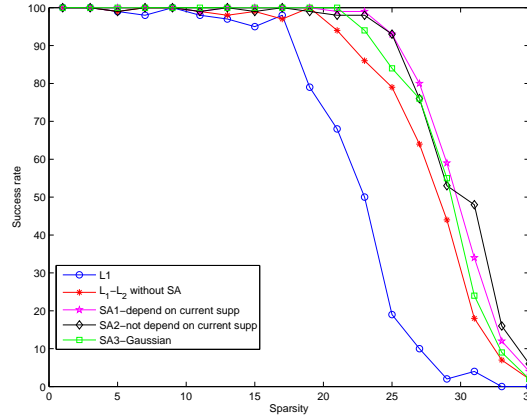


Figure 3: Plots of success rates of three SA algorithms: SA1-the support of the new state is within the current one, SA2-the new state does not depend on the current one, and SA3-the new state is obtained by adding Gaussian noise to the current one. The results of  $L_1$  and  $L_1 - L_2$  without SA are plotted as reference.

$N = 100, M = 1000$ , minimum separation is 2RL

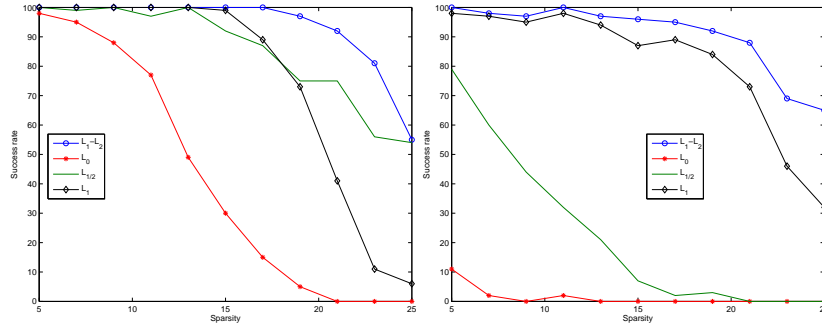


Figure 4: Plots of success rates as a function of sparsity for  $F = 5$  (left) and  $F = 20$  (right). Each metric is solved in a constrained optimization framework.

	$L_0$	$L_{1/2}$	$L_1$	$L_1 - L_2$
unconstrained $F = 5$	12.26	1.94	1.53	3.56
unconstrained $F = 20$	12.23	2.01	1.54	3.55
constrained $F = 5$	4.37	1.97	3.68	9.94
constrained $F = 20$	6.35	7.44	3.67	10.91

Table 2: Average computation time for each method at different settings.

the nominal wavelengths in the measurement  $J(\lambda)$  may not correspond exactly to those in the basis  $y_j(\lambda)$ . We must allow for small deformations  $v_j(\lambda)$  so that  $y_j(\lambda + v_j(\lambda))$  are all aligned with the data  $J(\lambda)$ . Taking into account wavelength misalignment, the data model becomes

$$J(\lambda) = \sum_j^M a_j \cdot y_j(\lambda + v_j(\lambda)) + \eta(\lambda). \quad (16)$$

Esser *et. al.* [10] construct an incremented dictionary by deforming each  $y_j$  with a set of possible deformations for the DOAS problem. Specifically, since it has been discovered that the deformations can be well approximated by linear functions, *i.e.*,  $v_j(\lambda) = p_j\lambda + q_j$ , all the possible deformations are enumerated by choosing  $p_j, q_j$  from two pre-determined sets  $\{P_1, \dots, P_K\}, \{Q_1, \dots, Q_L\}$ . Let  $Y_j$  be a matrix with each column be a deformed basis corresponding to  $y_j(\lambda)$ , *i.e.*,  $y_j(\lambda + P_k\lambda + Q_l)$  for  $k = 1, \dots, K$  and  $l = 1, \dots, L$ . Then the model (16) can be rewritten in terms of a matrix-vector form,

$$J = [Y_1, \dots, Y_M] \begin{bmatrix} \mathbf{a}_1 \\ \vdots \\ \mathbf{a}_M \end{bmatrix} + \eta, \quad (17)$$

where  $\mathbf{a}_j$  is a  $(KL)$ -dimensional column vector.

In our experiments, we generate such a dictionary by taking three given reference spectra  $y_j(\lambda)$  for the gases HONO, NO<sub>2</sub> and O<sub>3</sub> and deforming each by a set of linear functions. The represented wavelengths in nanometers are  $\lambda = 340 + 0.04038w$ ,  $w = 0, \dots, 1023$ , thus yielding each  $y_j \in \mathbb{R}^{1024}$ . We choose two pre-determined sets  $P_k = -1.01 + 0.01k$  ( $k = 1, \dots, 21$ ) and  $Q_l = -1.1 + 0.1l$  ( $l = 1, \dots, 21$ ), and hence there are a total of 441 linearly deformed references

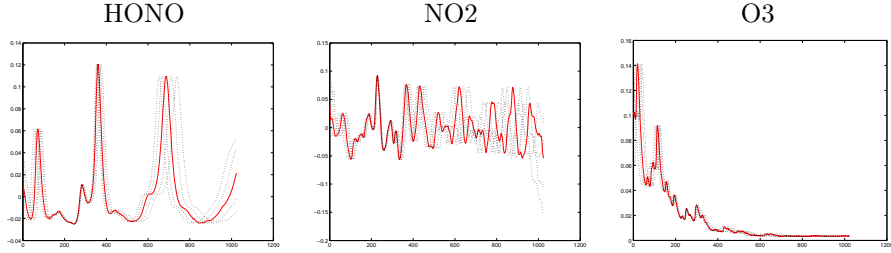


Figure 5: Each gas spectrum (a dictionary element) is plotted in red, while four deformed spectra (nearby dictionary elements) are in dotted black.

for each of the three groups. In Figure 5, we plot the reference spectra of these three gases together with four deformed examples. The coherence of the resulting dictionary is .9996.

To generate synthetic data  $J(\lambda) \in \mathbb{R}^W$ , we randomly select one element for each group with random magnitude plus additive zero mean Gaussian noise. Mimicking the relative magnitudes of a real DOAS dataset [12] after normalization of the dictionary, the random magnitudes are chosen to be at different orders with mean values of 1, 0.1, 1.5 for HONO, NO2 and O3 respectively. We consider four different noise levels, whose standard deviations  $\sigma$  are 0, .001, .005 and .01 respectively.

To solve the wavelength misalignment, the following minimization model is considered,

$$\arg \min_{\mathbf{a}_j} \|J - [Y_1, \dots, Y_M] \begin{bmatrix} \mathbf{a}_1 \\ \vdots \\ \mathbf{a}_M \end{bmatrix}\|^2, \quad (18)$$

$$\text{s.t. } \mathbf{a}_j \geq 0, \|\mathbf{a}_j\|_0 \leq 1 \quad j = 1, \dots, M. \quad (19)$$

The second constraint in (19) is to enforce each  $\mathbf{a}_j$  to have at most one non-zero element.  $\|\mathbf{a}_j\|_0 = 1$  indicates the existence of the gas with a spectrum  $y_j$  and its non-zero component corresponds to the selected deformation.

We consider a generic method to find sparse coefficients from the least square model (18). To enforce sparsity, we use  $L_1 - L_2$  and compare it with  $L_p$  for  $p = 1/2$ . When taking the non-negativity into account, we look at non-negative

noise std	NNLS	NN L1	L0	$L_1 - L_2$	$L_{1/2}$
0	0.00	0.90	0.00	0.0000	0.04
0.001	0.04	0.87	0.005	<b>0.003</b>	0.06
0.005	0.19	0.16	0.06	<b>0.058</b>	0.18
0.01	0.39	0.33	<b>0.20</b>	0.34	0.40

Table 3: Relative errors for each method under different amounts of noise. Each recorded value is the mean of 100 random realizations.

least square (NNLS) and non-negative constrained  $L_1$  (NN L1) as comparison. We use MATLAB’s `lsqnonneg` function, which is parameter free, to solve the NNLS. The constrained NN L1 is modelled as,

$$\min_{x \geq 0} \|x\|_1 \quad \text{such that} \quad \|Ax - b\| \leq \tau, \quad (20)$$

which can be solved by Bregman iteration [27]. We also compare with a direct  $L_0$  approach that takes advantages of the structured sparsity. This method is based on the idea of penalty decomposition [17], and therefore it requires a good initialization and slowly increases penalty parameter  $\rho^k$  in (3).

In Figures 6 and Figure 7, we plot the results of different methods in blue along with the ground truth solution in red for  $\sigma = 0$  and 0.005 respectively. Table 3 shows the relative errors between the reconstructed vector and the ground-truth under different amounts of noise. Each recorded value is the average of 100 random realizations. All the results demonstrate that  $L_1 - L_2$  is comparable to other methods without additional assumption on non-negativity or structured sparsity.

### 4.3 Image Denoising

An image denoising model [9] interprets an image as linear combinations of local overcomplete bases, where the vector of coefficients is *sparse*, so at any location only few bases contribute to the approximation. Suppose the discrete image patches of size  $\sqrt{n} \times \sqrt{n}$  pixels, ordered lexicographically as column vectors  $x \in \mathbb{R}^n$ , then the sparsity assumption corresponds to assuming the existence of a matrix  $D \in \mathbb{R}^{n \times K}$ , the “dictionary,” such that every image patch  $x$  can be

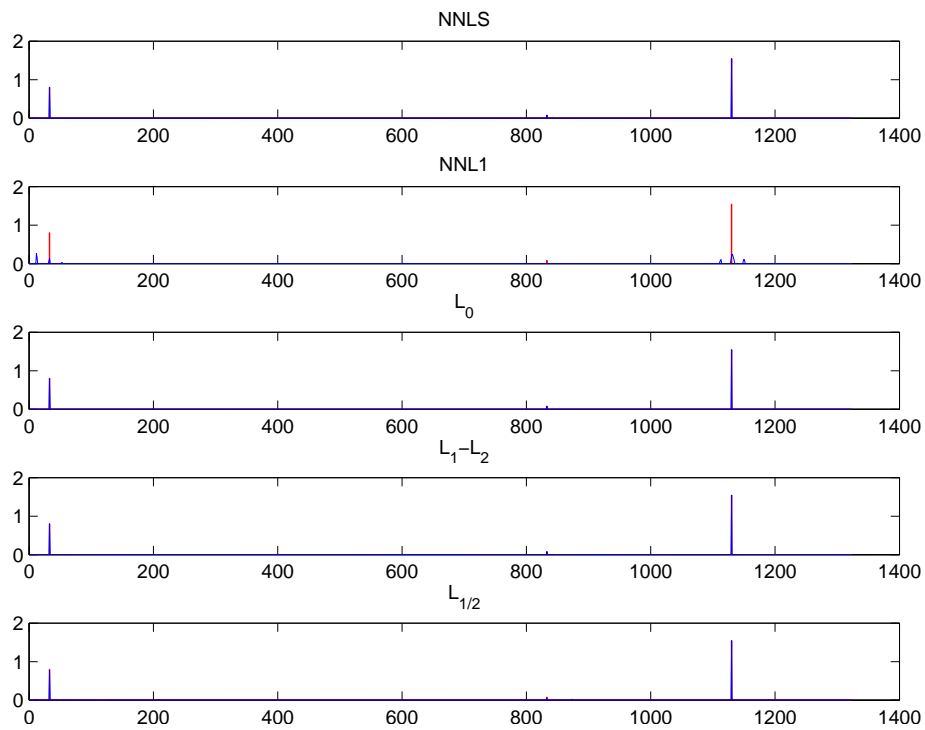


Figure 6: Method comparisons on synthetic DOAS data without noise. Computed coefficients (blue) are plotted on top of the ground truth (red).

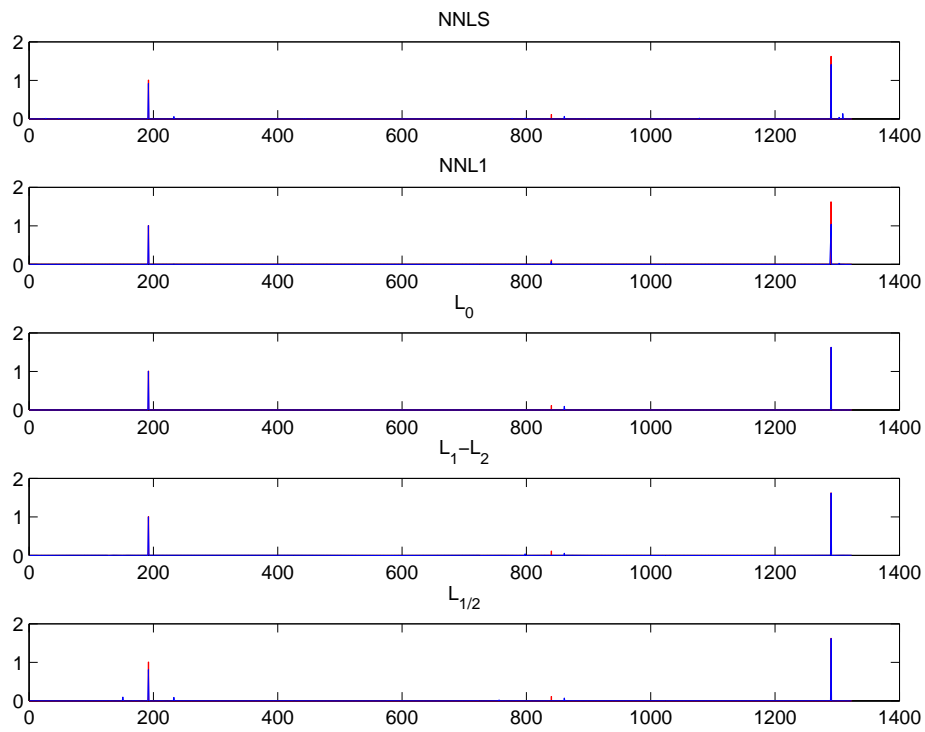


Figure 7: Method comparisons on synthetic DOAS data with additive noise  $\sigma = .005$ . Computed coefficients (blue) are plotted on top of the ground truth (red).

represented as a linear combination of its columns with a vector of coefficients that has small  $L_0$  norm. If we measure  $y$ , a version of  $x$  corrupted by additive Gaussian noise with standard deviation  $\sigma$ , then the maximum a-posteriori (MAP) estimator of the “denoised” patch  $x$  is given by  $D\hat{\alpha}$ , where

$$\hat{\alpha} = \arg \min_{\alpha} \|\alpha\|_0 \quad \text{s.t.} \quad \|D\alpha - y\|_2^2 \leq T, \quad (21)$$

where  $T$  is dictated by  $\sigma$ . If one wishes to encode a larger image  $X$  of size  $\sqrt{N} \times \sqrt{N}$  ( $N \gg n$ ), with a given dictionary  $D \in \mathbb{R}^{n \times K}$ , a natural approach is to use a block-coordinate relaxation.

$$\hat{X} = \arg \min_{X, \alpha_{ij}} \|X - Y\|_2^2 + \lambda \sum_{i,j} \|\alpha_{ij}\|_0 + \mu \sum_{i,j} \|D\alpha_{ij} - R_{ij}X\|_2^2. \quad (22)$$

The first term measures the fidelity between the measured image  $Y$  and its denoised (and unknown) version  $X$ . The second term enforces sparsity of each patch; the  $n \times N$  matrix  $R_{ij}$  extracts the  $(i, j)$ th block from the image. A simple denoising algorithm [9] goes as follows,

1. Given an overcomplete dictionary  $D$  and let  $X$  be noisy data  $Y$
2. Compute the coefficients  $\alpha_{ij}$  for each patch  $R_{ij}X$

$$\hat{\alpha}_{ij} = \arg \min_{\alpha} \|\alpha\|_0 \quad \text{s.t.} \quad \|D\alpha - R_{ij}X\|_2^2 \leq T. \quad (23)$$

3. Update  $X$  by

$$X = \frac{Y + \mu \sum_{i,j} R_{ij}^T D \alpha_{ij}}{I + \mu \sum_{i,j} R_{ij}^T R_{ij}}, \quad (24)$$

which is a simple averaging of shifted patches.

The aforementioned DCT basis (15) can be a candidate for such dictionary, but it is not suitable to represent natural image patches. Aharon *et. al.* propose a dictionary learning technique called K-SVD [1]. They construct a *global* dictionary that is trained from a large number of natural images. They also consider an *adaptive* dictionary by training on random samples of the noisy data so that the dictionary is more tailored to the data. The global dictionary is presented in Figure 8, which is used in our denoising experiments.

In the denoising model [9], the sparse coding step (23) is solved by orthogonal matching pursuit (OMP) [23], which is described in Algorithm 4. We can replace

OMP by enforcing sparse penalties  $L_1, L_p$  or  $L_1 - L_2$ . The results are presented in Figures 9 and Figure 10 for  $\sigma = 20, 30$  respectively. The peak-signal-to-noise (PSNR) is provided for quantitative comparison. We find  $L_0$  by OMP and its approximation  $L_p$  for  $p=1/4$  outperforms  $L_1$  and  $L_1 - L_2$  objectively in terms of PSNR. Perceptually,  $L_1 - L_2$  appears to leave fewer defects on Lena’s face and elsewhere than  $L_0$  and  $L_p$  with a rather close PSNR value. The reasons can be twofold. First, the dictionary is not as coherent as the previous examples, (its coherence is .9559). Second, there is no ground-truth sparsest solution in this case. Many solutions may look reasonable to human perception. Visually and objectively via PSNR,  $L_1 - L_2$  is always better than  $L_1$ .

---

**Algorithm 4** Orthogonal matching pursuit [23]

---

1. Start from vector  $b$  and initialize the residual  $R^i = b$  for  $i = 1$ .
2. Select the atom that maximizes the absolute value of the inner product of columns of  $A$  with  $R^i$ .
3. Form a matrix,  $\Phi$ , with previously selected atoms as the columns. Define the orthogonal projection operator onto the span of the columns of  $\Phi$

$$P = \Phi(\Phi^*\Phi)^{-1}\Phi^*$$

4. Apply the orthogonal projection operator to the residual and update

$$R^{i+1} = (I - P)R^i .$$

5. Let  $i = i + 1$  and go to Step 2; stop if  $s$  atoms are chosen.
- 

## 5 Conclusions and Future Work

In this paper, we studied  $L_1 - L_2$  as an alternative to  $L_1$  for sparse representation. We addressed several analytical properties of  $L_1 - L_2$  to promote sparsity. We proposed to compute sparse coefficients based on the difference of convex algorithm. Due to its nonconvex nature, we further considered a simulated annealing framework to approach a global solution. We have conducted an extensive study comparing sparse penalties,  $L_0, L_1, L_p, L_1 - L_2$ , and their numerical algorithms.

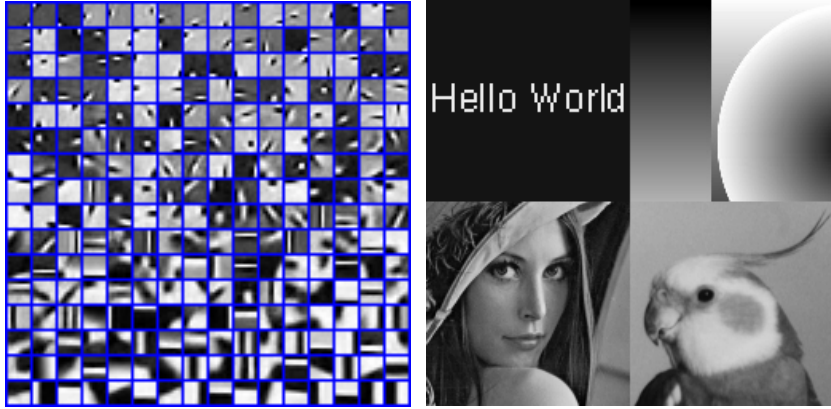


Figure 8: A global dictionary shown on the left is obtained from [1]. Each small blob is an  $8 \times 8$  patch, which corresponds to one column in the dictionary. A test image is shown on the right. It contains 4 sub images with different features.

Experiments have demonstrated that  $L_1 - L_2$  is better than  $L_1$  as a sparse regularization, especially when the sensing matrix or dictionary is highly coherent, and the DCA of  $L_1 - L_2$  is better than iterative reweighted strategies for  $L_p$  minimization.

For future work, we plan to pursue the following directions. As the DCA of  $L_1 - L_2$  is built upon  $L_1$ , it is interesting to study whether the support of  $L_1 - L_2$  solution is within the one of  $L_1$ . It has been noticed that not only does exact recovery of a sparse signal depend on the matrix, it also depends on the signal itself. We want to characterize exact sparse recovery in terms of minimum separation and/or Rayleigh length. Finally we want to investigate simulated annealing for this specific algorithm, such as how to advance to next step, how to determine the cooling strategy, and how to converge faster.

**Acknowledgments** - We thank Dr. Wotao Yin of the Department of Mathematics, UCLA, for providing us with Matlab codes of  $L_p$  minimization algorithms published in [7, 16].

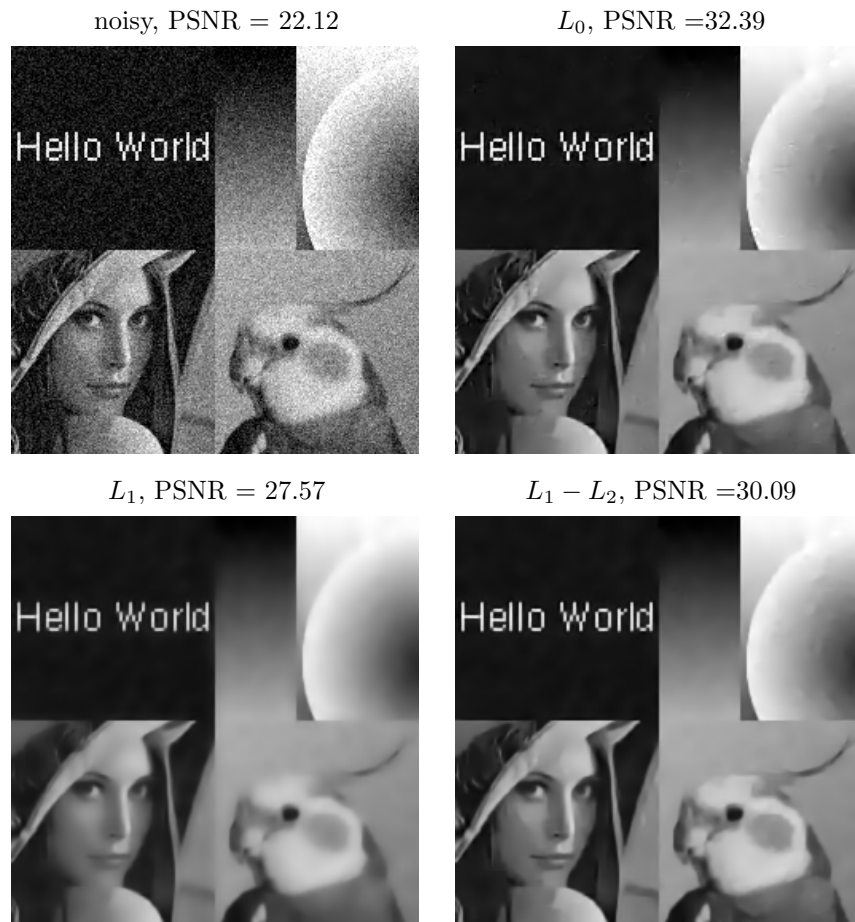


Figure 9: Denoising comparison with additive noise whose standard deviation is 20.

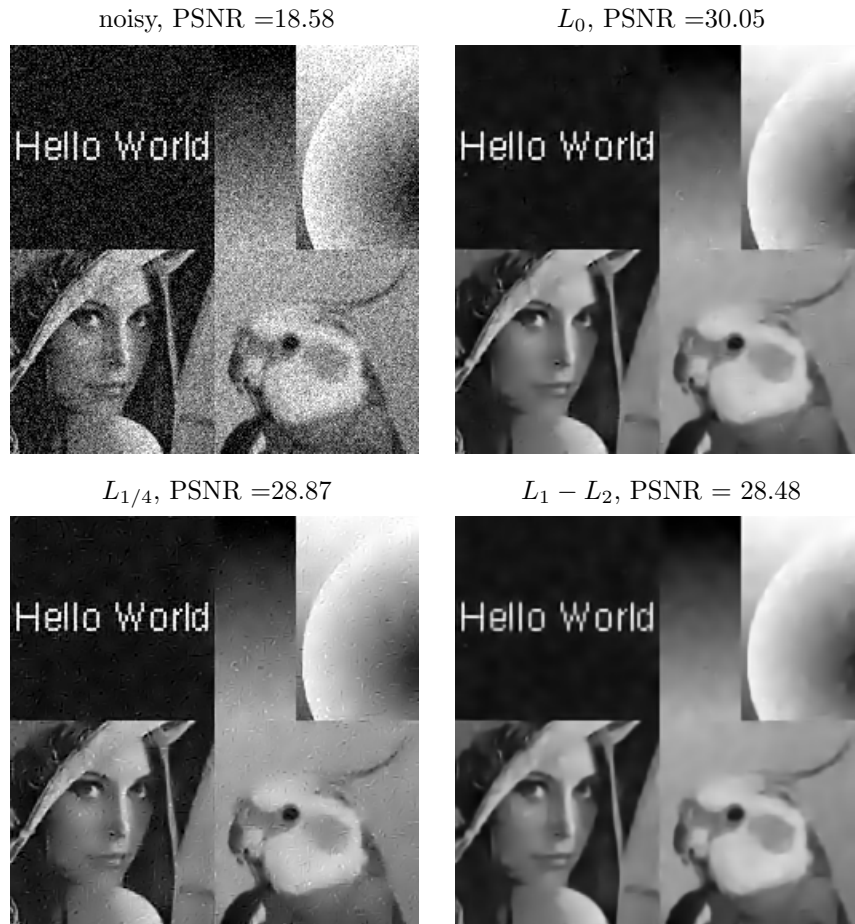


Figure 10: Denoising comparison with additive noise whose standard deviation is 30. There are more noticeable defects in  $L_0$  image than in  $L_1 - L_2$  image.

## References

- [1] M. Aharon, M. Elad, and A. Bruckstein. K-SVD: An algorithm for designing overcomplete dictionaries for sparse representation. *IEEE Trans. Signal Processing*, 54(11):4311–4322, 2006.
- [2] S. Boyd, N. Parikh, E. Chu, B. Peleato, and J. Eckstein. Distributed optimization and statistical learning via the alternating direction method of multipliers. *Found. Trends Mach. Learn.*, 3(1):1–122, January 2011.
- [3] E. Candès, Y. Elder, D. Needle, and P. Randall. Compressed sensing with coherent and redundant dictionaries. *Applied Comput. Harmonic Anal.*, 31:59–73, 2011.
- [4] E. J. Candès and C. Fernandez-Granda. Super-resolution from noisy data. *to appear in Journal of Fourier Analysis and Applications*, August 2013.
- [5] E. J. Candès and T. Tao. Decoding by linear programming. *IEEE Trans. Inf. Th.*, 51(12):4203–4215, 2005.
- [6] P. Carnevali, L. Coletti, and S. Patarnello. Image processing by simulated annealing. *IBM Journal of Research and Development*, 29(6):569–579, 1985.
- [7] R. Chartrand and W. Yin. Iteratively reweighted algorithms for compressive sensing. In *International Conference on Acoustics, Speech, and Signal Processing*, pages 3869–3872, 2008.
- [8] D. Donoho and M. Elad. Optimally sparse representation in general (nonorthogonal) dictionaries via  $l_1$  minimization. *Proc. Nat. Acad. Scien. USA*, 100:2197–2202, March 2003.
- [9] M. Elad and M. Aharon. Image denoising via sparse and redundant representations over learned dictionaries. *IEEE Trans. Image Process.*, 15(12):3736–3745, 2006.
- [10] E. Esser, Y. Lou, and J. Xin. A method for finding structured sparse solutions to non-negative least squares problems with applications. *SIAM Journal on Imaging Sci.*, 6(4):2010–2046, 2013.

- [11] A. Fannjiang and W. Liao. Coherence pattern-guided compressive sensing with unresolved grids. *SIAM J. Img. Sci.*, 5(1):179–202, February 2012.
- [12] B. Finlayson-Pitts. Unpublished data. Provided by L. Wingen, 2000.
- [13] S. Geman and D. Geman. Stochastic relaxation, Gibbs distributions, and the Bayesian restoration of images. *Pattern Analysis and Machine Intelligence, IEEE Transactions on*, (6):721–741, 1984.
- [14] B. Gidas. Nonstationary Markov chains and convergence of the annealing algorithm. *Journal of Statistical Physics*, 39(1-2):73–131, 1985.
- [15] S. Kirkpatrick, C. D. Gelatt, and M. P. Vecchi. Optimization by simulated annealing. *Science*, 220(4598):671–680, 1983.
- [16] M. J. Lai, Y. Xu, and W. Yin. Improved iteratively reweighted least squares for unconstrained smoothed lq minimization. *SIAM Journal on Numerical Analysis*, 5(2):927–957, 2013.
- [17] Z. Lu and Y. Zhang. Penalty decomposition methods for L0-norm minimization. *preprint*, 2010.
- [18] B. K. Natarajan. Sparse approximate solutions to linear systems. *SIAM J. on computing*, pages 227–234, 1995.
- [19] B. Olshausen and D. Field. Sparse coding with an overcomplete basis set: A strategy employed by v1? *Vision Research*, 37:3311–3325, 1997.
- [20] U. Platt and J. Stutz. *Differential Optical Absorption Spectroscopy: Principles and Applications*. Springer, 2008.
- [21] P. D. Tao and L. T. H. An. Convex analysis approach to d.c. programming: Theory, algorithms and applications. *Acta Mathematica Vietnamica*, 22(1):289–355, 1997.
- [22] R. Tibshirani. Regression shrinkage and selection via the lasso. *J. Royal. Statist. Soc B.*, 58(1):267–288, 1996.
- [23] J. Tropp. Greed is good: Algorithmic results for sparse approximation. *IEEE Trans. Inform. Theory*, 50:2231–2242, 2004.

- [24] F. Xu and S. Wang. A hybrid simulated annealing thresholding algorithm for compressed sensing. *Signal Processing*, 93:1577–1585, 2013.
- [25] P. Yin, E. Esser, and J. Xin. Ratio and difference of  $l_1$  and  $l_2$  norms and sparse representation with coherent dictionaries. Technical report, 2013. UCLA CAM Report [13-21].
- [26] P. Yin, Y. Lou, Q. He, and J. Xin. Minimization of  $l_1 - l_2$  for compressed sensing. Technical report, 2014. UCLA CAM Report [14-01].
- [27] W. Yin, S. Osher, D. Goldfarb, and J. Darbon. Bregman iterative algorithms for  $l_1$  minimization with applications to compressed sensing. *SIAM J. Imaging Sci*, 1:143–168, 2008.